Modular Synthesis of Functional Nanoscale Coordination Polymers

Wenbin Lin[*], **William J. Rieter**, and **Kathryn M. L. Taylor**
Department of Chemistry, CB#3290, University of North Carolina, Chapel Hill, NC 27599, USA

Abstract

The coordination-directed assembly of metal ions and organic bridging ligands has afforded a variety of bulk-scale hybrid materials with promising characteristics for a number of practical applications, such as gas storage and heterogeneous catalysis. Recently, so-called coordination polymers have emerged as a new class of hybrid nanomaterials. Herein, we highlight advances in the syntheses of both amorphous and crystalline nanoscale coordination polymers. We also illustrate how scaling down these materials to the nano-regime has enabled their use in a broad range of applications including catalysis, spin-crossover, templating, biosensing, biomedical imaging, and anticancer drug delivery. These results underscore the exciting opportunities of developing next-generation functional nanomaterials based on molecular components.

Keywords

coordination polymers; metal-organic; frameworks; nanoparticles; biomedical imaging; drug delivery

1. Introduction

Technological advancements have led to new and exciting applications for materials that might have once been thought inconceivable. This holds particularly true for the rapidly developing field of nanotechnology. The unique size-dependent properties of materials on the nanometer-scale have led to their applications in many areas, including catalysis,[1] wavelength-tunable lasers,[2] solar cells,[3] bioimaging,[4] and drug delivery.[5] While the vast majority of nanomaterials are either purely inorganic or organic in composition, the combination of metal and organic components at a molecular level has recently afforded a new class of highly tailorable hybrid nanomaterials known as nanoscale coordination polymers.

Coordination polymers or metal-organic frameworks are built from metal ions or metal ion clusters that have two or more vacant coordination sites and polydentate bridging ligands. Prussian blue and mixed metal cyanometallates are the classic examples of coordination polymers.[6] Numerous reports on the syntheses and characterization of cyanometallate nanoparticles have been published over the last decade (Figure 1),[7] and they too exhibit

[*]Fax: (+1)919-962-2388, wlin@unc.edu.

unique size dependent properties such as suparamagnetism,[7a] photo-induced superparamagnetism,[7b] and spin-glass-like behaviour.[7c] Coordination polymers however are not limited to the cyanometallates, and can be synthesized from a wide range of metal and organic building blocks. The tunable nature of coordination polymers has allowed them to be engineered for a number of bulk-scale applications, including gas storage,[8a] catalysis,[8b] and nonlinear optics.[8c] Their scale-down to the nanometer-regime will vastly expand the scope of cyanometallate nanoparticles and lead to a new generation of functional nanostructures. In this minireview, we present recent advances in the syntheses of nanoscale coordination polymers, and illustrate the application of this exciting new class of nanomaterials in many areas ranging from heterogeneous catalysis to anticancer drug delivery.

2. Synthesis of Nanoscale Coordination Polymers

2.1. Classification of Nanoscale Coordination Polymers

Nanoscale coordination polymer particles can be divided into two main classes based on their structural regularity/crystallinity: the amorphous class that is denoted as NCPs and the crystalline class known as nanoscale metal-organic frameworks (NMOFs). NCPs typically adopt a spherical morphology to minimize the interfacial free energy between the particles and solvent. On the other hand, the morphologies of NMOFs are controlled by both the intrinsic crystal structures and their interactions with the solvent molecules. NMOFs tend to adopt well-defined non-spherical morphologies, suggesting the dominance of crystal lattice energy over the particle/solvent interactions. The crystalline nature of NMOFs allows for an exact understanding of their compositions and structures, and greatly facilitates the delineation of composition, structure, and property inter-relationships in this class of nanostructures.

2.2. Synthesis of Amorphous Nanoscale Coordination Polymers

NCPs are generally synthesized by exploiting the insolubility of the particles in a given solvent system. Wang et al. reported the first synthesis of non-cyanometallate NCPs in 2005.[9] The authors discovered that submicrometer-scale spherical colloids could be prepared by simply mixing H_2PtCl_6 and *p*-phenylenediamine in an aqueous solution. From a ~0.50 mM solution of the reagents they isolated monodisperse spheres of ~420 nm in diameter. This work took advantage of the fact that the product from the reaction between the two components has a very low solubility in water.

Sweigart and Son also used this approach to formulate particles consisting of [(η^6-1,4-hydroquinone)Rh(COD)]$^+$ linkers and Al^{3+} metal ion connectors.[10] Addition of Al(O*i*Pr)$_3$ to a solution of the organo-rhodium complex in THF immediately led to the precipitation of nanoparticles with an average diameter of 340 nm (Scheme 1). They further showed that the particle sizes increased as the reagent concentrations increased, suggesting the influence of the particle growth rates on their sizes. This synthetic strategy is reminiscent of those used for the synthesis of highly enantioselective zirconium phosphonate-based heterogeneous asymmetric catalysts with ill-defined morphologies.[11]

Mirkin and co-workers described a different approach toward NCPs by precipitating particles from a precursor solution of the components via the addition of a poor solvent.[12] NCPs based on metal and homochiral carboxylate-functionalized bis-metallo-tridentate Schiff base (BMSB) building blocks were, for example, prepared by adding a poor, initiating solvent such as diethyl ether or pentane to a solution of the metal and BMSB components in pyridine (Scheme 2). While slow diffusion of the poor solvent into the precursor solution resulted in micron-sized particles, its rapid addition gave much smaller NCPs. These results were significant because they showed the growth processes could be quenched at an early stage of the reaction.

Lin et al. recently used a similar strategy to formulate NCPs composed of the anticancer drug disuccinatocisplatin (DSCP) and Tb^{III}.[13] In the synthesis, the pH of an aqueous solution of $TbCl_3$ and di(methylammonium) DSCP was adjusted to ~5.5 with dilute NaOH (Scheme 3). Methanol was then quickly poured into the precursor solution to induce the formation of NCPs with a diameter of 58 ± 11.3 nm. Careful control of the pH of the aqueous precursor solution was critical for the successful and reproducible synthesis of NCPs in this system.

NCPs have also been prepared from the assembly of 1-d coordination oligomers. These NCPs are distinct because of the initial formation of defined linear chain complexes (high oligomers) in solution. For instance, Maeda and co-workers noted that treatment of dipyrrin "dimers" with $Zn(OAc)_2$ in THF resulted in a color change indicative of the coordination between Zn ions and dipyrrin units (Scheme 4).[14] Uniform nanoparticles were obtained when an initial concentration of the components was carefully chosen, presumably as a result of the assembly of pre-formed oligomeric species into NCPs. They also studied the structural effects of the dimers on nanoparticle formation, and proposed a multi-step sequence for NCP particle formation that is akin to the protein folding process.

Similarly, Ruiz-Molina and co-workers prepared NCPs based on 1-d oligomers by rapidly adding water to a solution of $Co(OAc)_2$, 3,5-di-*tert*-butyl-1,2-catechol (dbcat), and 1,4-bis(imadizol-1-ylmethyl)benzene (bix) in an ethanol/water mixture (Figure 2).[15] The size of the particles was tuned from 76 ± 9 nm to 204 ± 13 nm by varying the rate at which the water was added to precipitate the particles from 50 to 0.07 mL s^{-1}. These results again illustrate the ability to control the particle growth processes by quenching with a poor solvent.

2.2. Synthesis of Nanoscale Metal-Organic Frameworks

The amorphous nature of NCPs prohibits a detailed understanding of these systems at a molecular level, and can lead to additional variability in the compositions, size distributions, and morphologies between different experiments. Several distinct approaches have recently been developed for the synthesis of crystalline NMOFs, including water-in-oil microemulsions, surfactant-mediated hydrothermal syntheses, and high-temperature routes. Single crystal X-ray diffraction studies of the bulk MOFs provide an unequivocal understanding of the composition and structure of the nanoparticles, greatly facilitating characterization of NMOFs.

The ability to control the sizes of cyanometallate nanoparticles using water-in-oil microemulsions provided the inspiration to utilize this methodology for NMOF synthesis. Water-in-oil, or reverse, microemulsions are highly tailorable systems that consist of nanometer-sized water droplets stabilized by a surfactant in a predominantly organic phase. The micelles in the microemulsion essentially act as "nanoreactors" that assist in controlling the kinetics of particle nucleation and growth. The size and number of micelles within the microemulsion can be tuned by varying the water to surfactant ratio (W).

Lin et al. prepared $Ln_2(BDC)_3(H_2O)_4$ NMOFs (where $Ln = Eu^{3+}$, Gd^{3+}, or Tb^{3+} and BDC = 1,4-benzenedicarboxylate) by reacting $LnCl_3$ and di(methylammonium) BDC in the cationic cetyltrimethylammonium bromide (CTAB)/isooctane/1-hexanol/water microemulsion system (Figure 3a–b).[16] Nanorods of fairly uniform size were isolated in high yield. By varying the W value from 5 to 10, the sizes of the nanorods could be tuned from ~125 nm in length by ~40 nm in width to ~2 μm in length by ~100 nm in width. The rod-like shape of the nanoparticles reflects the anisotropies associated with the growth of the nanocrystals. Higher W values lead to particles with higher aspect ratios due to a decrease of nucleation sites within the microemulsion. Moreover, the particle size decreased as the reactant concentrations were increased, presumably because more micelles were occupied by the reactants to generate more nucleation sites, leading to a reduction of particle sizes.

$[Ln(iBTC)(H_2O)_3]\cdot H_2O$ NMOFs (where $iBTC$ = 1,2,4-benzenetricarboxylate) were similarly prepared by stirring a mixture of $LnCl_3$ and tri(methylammonium) $iBTC$ in a CTAB/isooctane/1-hexanol/water microemulsion mixture (Figure 3c–d). Nanoplates with an average diameter of ~100 nm were isolated from a microemulsion of W=15 when excess metal was used in the reaction.

NMOFs based on Mn^{2+} connectors and BDC and 1,3,5-benzenetricarboxylate (BTC) bridging ligands were also synthesized in reverse microemulsions (Figure 4).[17] NMOFs of $Mn(BDC)(H_2O)_2$ were isolated as long rods, with a structure corresponding to a known crystalline phase. NMOFs of $Mn_2(BTC)_3(H_2O)_6$ were isolated as crystalline spiralling rods, but their structure did not correspond to any known phase of Mn-BTC-based MOFs.

Using a similar microemulsion-based method, Coronado et al. recently prepared spherical nanoparticles based on a 1-d polymeric structure with the formula $[Fe(Htrz)_2(trz)](BF_4)$ (where Htrz is 1,2,4-1H-triazole).[18] Nanoparticles with a diameter of 11 ± 5 nm were obtained by mixing $Fe(BF_4)_3\cdot H_2O$, behenic acid, and Htrz in a microemulsion composed of the anionic surfactant sodium dioctyl sulfosuccinate (NaAOT), octane, and water.

While the room temperature microemulsion synthesis has afforded a number of NMOFs with various metal/ligand combinations, it has also led to amorphous gel-like materials for some, presumably as a result of the rapid and irreversible metal to ligand bond formation. Lin et al. recently developed a surfactant-mediated hydrothermal method for the synthesis of NMOFs.[20] Elevated temperatures can alter the relative kinetics for nucleation and nanocrystal growth, favoring the formation of uniform nanomaterials under hydrothermal conditions.

NMOFs of the composition $Gd_2(BHC)(H_2O)_6$ were prepared by heating a mixture of hexa(methylammonium) benzenehexa-carboxylate (BHC) and $GdCl_3$ in a microemulsion composed of CTAB, 1-hexanol, heptane, and water at 120 °C.[20] The resulting block-like particles with dimensions of ~ 25×50×100 nm corresponded to a known crystalline La analog with the fluorite network topology (Figure 5).

Interestingly, nanorods of $[Gd_2(BHC)(H_2O)_8]\cdot 2H_2O$ were obtained by reacting $GdCl_3$ and mellitic acid (BHC-H_6) in the same microemulsion system at 60 °C in a microwave reactor.[20] Electron micrographs showed that the nanorods were ~100–300 nm in diameter and several microns in length (Figure 6a–b). X-ray structure studies revealed that each Gd center coordinates to two chelating carboxylates and one monodentate carboxylate from three different BHC ligands and four water molecules. The BHC ligand acts as a six-connected node whereas the Gd center acts as a three-connected node to lead to a 3D framework with the rutile network topology (Figure 6c–e).

The synthesis of two different NMOFs based on the Gd/BHC building blocks is a result of the different metal-ligand coordination modes. The coordination isomerism observed in this system is pH but not temperature dependent. This work illustrates the ability to synthesize different NMOFs from the same metal/ligand combination by exploiting the versatile metal-ligand coordination modes.

Jung and Oh recently reported a solvothermal method for NMOF synthesis and closely monitored the particle morphological transformation during the synthesis (Figure 7).[21] A solution of *N,N′*-phenylenebis(salicylideneimine)dicarboxylic acid in DMSO was added to a DMF solution containing two equiv of $Zn(OAc)_2$. One equiv of the Zn ions coordinates to the salen pocket while the other connects the metalloligands. The resulting solution was heated at 120 °C for 60 min, over which time they observed the transformation of nanowires into nanocubes via aggregation and intrastructural fusion. They also demonstrated that the sizes of the cubes could be tuned by varying the reaction conditions: smaller particles were obtained when the solubility of the nanowires was decreased by either lowering the temperature or using a poorer solvent mixture.

3. Applications of Nanoscale Coordination Polymers

Since nanoscale coordination polymers can be built from a wide selection of metal ions and an infinite number of organic bridging ligands, they can be engineered with an unprecedented range of compositions and properties. This high degree of tailorability has led to the synthesis of a number of NCP and NMOF materials. More importantly, they have been shown to exhibit interesting characteristics for a variety of applications, including catalysis, spin-crossover, templating, biological sensing and multimodal biomedical imaging, and drug-delivery.

3.1. Heterogeneous Catalysis

Heterogeneous catalysts often display size dependent physical and chemical properties since the activity depends on surface area and substrate transport. The immobilization of organometallic complexes via their incorporation into self-supported networks, such as

NCPs, is a particularly promising strategy to formulate materials with a high density of catalytically active sites. Sweigart and Son's organometallic nanocatalyst (ON) based on the $[(\eta^4\text{-}1,4\text{-quinone})Rh(COD)]^-$ linker unit was shown to catalyze the stereoselective polymerization of phenylacetylene.[10] The size dependent catalytic properties of ONs are clearly illustrated in Table 1. Smaller particles yielded longer poly(phenylacetylene) polymers owing to increased catalytic activity. Moreover, the ONs were much more stereoselective than the molecular organo-rhodium catalyst.

3.2. Spin-Crossover

Spin-crossover is a phenomenon whereby a material transitions from a low-spin configuration to a low-lying metastable high-spin configuration through external stimuli such as temperature or light irradiation. Octahedral Fe^{II} compounds with the $3d^6$ electronic configuration are among the most extensively studied spin-crossover systems. The $[Fe(Htrz)_2(trz)](BF_4)$ nanoparticles prepared by Coronado et al. displayed a thermally-induced low to high spin transition almost identical to that reported for the bulk sample (Figure 8).[18] This transition is accompanied by a drastic color change from deep purple/red to light pink or white, which has previously been utilized in the development of write/read technologies. Similar spin-crossover behavior was seen in the NCPs prepared by Ruiz-Molina et al.[15] The nanoparticles with a low spin-$[Co^{III}(3,5\text{-dbsq})(3,5\text{-dbcat})]$ configuration could be thermally transformed to the high spin-$[Co^{II}(3,5\text{-dbsq})_2]$ material. More recently, Gaspar, Real, and co-workers described the synthesis of bimetallic NMOFs $[Fe(pz)Pt(CN)_4]\cdot xH_2O$ (pz is pyrazine, x=1 or 2.5) that exhibit magnetic, optical, and structural bistability near room temperature.[19] The bistability of these spin-crossover nanoparticles makes them attractive candidates for active components in a variety of multifunctional materials, and particularly in memory devices.

3.3. Templating with NMOFs

Core-shell nanostructures can exhibit interesting properties that result from both the templating core and the coating layer. Lin et al. demonstrated the utility of NMOFs as a template for the synthesis of novel core-shell nanostructures.[22] NMOFs were first coated with polyvinylpyrollidone (PVP) to reduce particle aggregation in solution. The PVP-functionalized intermediates were then treated with tetraethylorthosilicate (TEOS) in an ammonia/ethanol mixture to give nanocomposites with a NMOF core and a silica shell. The silica shell thickness could be tuned by varying the reaction time or by adjusting the amount of TEOS added to the reaction mixture.

The NMOF core could be completely removed (via dissolution) at low pH to afford hollow silica shells with varied thickness and aspect ratios. Since the morphologies of NMOFs can be controlled by exploiting the energetics of different crystallographic faces, such a templating approach can be used to produce interesting nanoshells that are not accessible with presently available methods. For example, silica nanoshells with a very high aspect ratio of 40 were synthesized using Gd-BDC NMOF as the template.

The silica shell of such nanocomposites also significantly stabilized the NMOF core against dissolution. The dissolution curves for as-synthesized and silica-coated Gd-BDC NMOFs

had a zeroth-order rate constant of 0.143 and 0.084 μM/h at pH=4, respectively. These results indicate that the rates of cargo release from such core-shell nanostructures can be readily controlled by taking advantage of slow diffusion of metal and organic constituents through the silica shell.

Silica as a surface coating offers several additional advantages, including enhanced water dispersibility, biocompatibility, and the ease of further functionalization with a variety of silyl-derived molecules. As shown below, the nanocomposites with NCP or NMOF cores and silica shells have been used for biosensing, multimodal imaging, and anticancer drug delivery.

3.4. Biosensing and Multimodal Imaging

Gd- and Mn-based NMOFs were shown to enhance image contrast in magnetic resonance imaging (MRI). MRI is a powerful non-invasive diagnostic technique that can differentiate normal tissue from diseased tissue based on variations of the NMR water proton signals. These variations arise from differences in water density, tissue environment, and/or nuclear relaxation rates. Complexes of highly paramagnetic metal ions, such as Gd^{3+} and Mn^{2+}, are often administered to enhance image contrast by increasing the rate of water proton relaxation. By incorporating the metal ions or metal complexes into nanoparticles the rate of relaxation can be further increased due to reduced rotational diffusion of the contrast agent. For example, the $Gd_2(BDC)_3(H_2O)_4$ nanorods ~100 nm in length by 40 nm in diameter display a longitudinal relaxivity (r_1) value of 35.8 $mM^{-1}s^{-1}$ in an aqueous xanthan gum suspension.[16] This value is almost an order of magnitude higher than that obtained with the commercially available T_1-weighted contrast agent Omniscan. More importantly, the relaxivities on a per particle basis are extraordinarily high due to the presence of a very large number of Gd^{3+} centers in each particle, which would potentially allow them to be effective site-specific contrast agents when conjugated to the appropriate targeting moieties.

NCPs and NMOFs can also be rendered luminescent by incorporating emissive metal ions or organic fluorophores (Figure 10). Gd NMOFs can be doped with the emissive lanthanide ions Eu^{3+} or Tb^{3+} to afford luminescent nanoparticles.[16] The organic linkers such as benzenedicarboxylic acid act as antenna to absorb light and transfer its excitation energy to the lanthanide ions. NCPs can be built from luminescent organic or organometallic linkers that have a high absorption coefficient and thus obviate the need of an antenna. The M-BMSB linker prepared by Mirkin gave an emission peak at ~ 600 nm (λ_{ex} = 420 nm), and the M-BMSB-M′ particles were highly luminescent under ultraviolet irradiation.[12] The optical properties of these materials could also be fine-tuned by changing the ancillary ligands coordinating to the metal centers.

NMOF-silica core-shell nanostructures were used for the ratiomeric detection of the dipicolinic acid (DPA), a major constituent of spore-forming bacteria (such as Anthrax), in solution (Figure 11). Eu-doped $Gd_2(BDC)_3(H_2O)_4$@SiO_2 core-shell nanoparticles were functionalized with a silylated Tb-EDTA moiety.[22] While the Eu-doped NMOFs were inherently luminescent, the sensitized emission from Tb was dependant upon the complexation of DPA. The Tb luminescence signal thus provided a sensitive probe for DPA

detection, while the Eu emission from the NMOF core acted as a non-interfering internal calibration.

NMOF-silica nanostructures were recently functionalized with rhodamine B and a targeting peptide for cancer imaging. Confocal fluorescence microscopy and MRI studies showed that the cyclic(RGDfK)-targeted particles with the $Mn_3(BTC)_2(H_2O)_6$ NMOF core and silica shell exhibited enhanced uptake by angiogenic human colon carcinoma (HT-29) cells as compared to non-targeted particles (Figure 12).[17] NCPs and NMOFs thus provide an interesting platform for designing multifunctional nanomaterials for biosensing and biomedical imaging.

3.5. Drug Delivery

As described in Section 3.3, the silica shell in the NMOF-silica nanocomposite stabilized the NMOF core and allowed for control of the cargo release rate by varying the silica shell thickness. Lin et al. used this strategy to effectively deliver anticancer drugs.[13] The NCPs based on the DSCP and Tb^{III} building blocks were first coated with a silica shell. The half-life for the release of DSCP, an analog of the anticancer drug cisplatin, from NCPs of the composition $Tb_2(DSCP)_3(H_2O)_{12}$ could be tuned from ~5.5 h to 9 h by increasing the shell thickness from ~2 nm to ~7 nm. In comparison, the as-synthesized NCPs had a $t_{1/2}$ for dissolution of only 1 h. *In vitro* cytotoxicity assays showed that the Pt-based NCP particles displayed anticancer efficacies superior to the cisplatin standards (Figure 13). These results were significant because they clearly demonstrated the feasibility of using NCPs as delivery vehicles for clinically relevant cargoes.

4. Summary and Outlook

The past few years have witnessed the synthesis of nanoscale coordination polymers of both amorphous (NCP) and crystalline (NMOF) nature. They have been synthesized by a variety of techniques, including precipitation by combining metal and organic components, precipitation via the addition of a poor solvent, microemulsion synthesis, surfactant-mediated synthesis, and hydrothermal synthesis. New synthetic strategies are still needed in order to take full advantage of the limitless number of possible formulations of NCPs and NMOFs.

The utility of many of the NCPs and NMOFs has been demonstrated in a number of interesting applications, such as catalysis, spin-crossover, templating, biosensing, biomedical imaging, and anticancer drug delivery. This class of nanomaterials allows for the exploration of many other applications by taking advantage of the ability to systematically tune the compositions via judicious choice of building blocks. A specific area that has received little attention, but could provide great advantages, is the scaling down of catalytically active MOFs to the nano-regime. This would greatly alter the diffusion kinetics, resulting in much more efficient heterogeneous catalysts. We believe that modular synthesis of nanoscale coordination polymers can lead to a new generation of functional nanomaterials based on molecular components.

Acknowledgments

References

1. Haruta M. Chem. Rev. 2003; 3:75–87.

2. Klimov VI, Ivanov SA, Nanda J, Achermann M, Bezel I, McGuire JA, Piryatinski A. Nature. 2007; 447:441–446. [PubMed: 17522678]

3. a) Gur I, Fromer NA, Geier ML, Alivisatos AP. Science. 2005; 310:462–465. [PubMed: 16239470] b) Grätzel M. Inorg. Chem. 2005; 44:6841–6851. [PubMed: 16180840]

4. a) Gao X, Cui Y, Levenson RM, Chung LW, Nie S. Nature Biotechnol. 2004; 22:969–976. [PubMed: 15258594] b) Sönnichsen C, Reinhard BM, Liphardt J, Alivisatos AP. Nature Biotechnol. 2005; 23:741–745. [PubMed: 15908940] c) Skrabalak SE, Chen J, Sun Y, Lu X, Au L, Cobley CM, Xia Y. Acc. Chem. Res. 2008

5. a) Vallet-Regí M, Balas F, Arcos D D. Angew. Chem. Int. Ed. 2007; 46:7548–7558.b) Zhang L, Gu FX, Chan JM, Wang AZ, Langer RS, Farokhzad OC. Clin Pharmacol Ther. 2008; 83:761–769. [PubMed: 17957183]

6. Entley WR, Girolami GS. Science. 1995; 268:397–400. [PubMed: 17746547]

7. a) Vaucher S, Li M, Mann S. Angew. Chem. Int. Ed. 2000; 39:1793.b) Vaucher S, Fielden J, Li M, Dujardin E, Mann S. Nano Letters. 2002; 2:225–229.c) Catala L, Gacoin T, Boilot JP, Riviere E, Paulsen C, Lhotel E, Mallah T. Adv. Mater. 2003; 15:826.d) Uemura T, Kitagawa S. J. Am. Chem. Soc. 2003; 125:7814–7815. [PubMed: 12822995] e) Fiorito PA, Goncales VR, Ponzio EA, de Torresi SIC. Chem. Comm. 2005:366–368. [PubMed: 15645039] f) Taguchi M, Yamada K, Suzuki K, Sato O, Einaga Y. Chem. Mater. 2005; 17:4554–4559.g) Uemura T, Kitagawa S. Chem. Lett. 2005; 34:132–137.

8. a) Kitagawa S, Kitaura R, Noro S. Angew. Chem. Int. Ed. 2004; 43:2334–2375.b) Wu C, Lin W. Angew. Chem. Int. Ed. 2007; 46:1075.c) Evans OR, Lin W. Acc. Chem. Res. 2002; 35:511. [PubMed: 12118990]

9. Sun XP, Dong SJ, Wang EK. J. Am. Chem. Soc. 2005; 127:13102–13103. [PubMed: 16173711]

10. Park KH, Jang K, Son SU, Sweigart DA. J. Am. Chem. Soc. 2006; 128:8740–8741. [PubMed: 16819862]

11. a) Hu A, Ngo HL, Lin W. Angew. Chem. Int. Ed. 2003; 42:6000–6003.b) Hu A, Ngo HL, Lin W. J. Am. Chem. Soc. 2003; 125:11490–11491. [PubMed: 13129339]

12. a) Oh M, Mirkin CA. Nature. 2005; 438:651–654. [PubMed: 16319888] b) Oh M, Mirkin CA. Angew. Chem. Int. Ed. 2006; 45:5492–5494.

13. Rieter WJ, Pott KM, Taylor KML, Lin W. J. Am. Chem. Soc. 2008

14. Maeda H, Hasegawa M, Hashimoto T, Kakimoto T, Nishio S, Nakanishi T. J. Am. Chem. Soc. 2006; 128:10024–10025. [PubMed: 16881626]

15. Imaz I, Maspoch D, Rodriguez-Blanco C, Perez-Falcon JM, Campo J, Ruiz-Molina D. Angew. Chem. Int. Ed. 2008; 47:1857–1860.

16. Rieter WJ, Taylor KM, An H, Lin W, Lin W. J Am. Chem. Soc. 2006; 128:9024–9025. [PubMed: 16834362]

17. Taylor KML, Rieter WJ, Lin W. J. Am. Chem. Soc. under revision.

18. Coronado E, Galan-Mascaros JR, Monrabal-Capilla M, Garcia-Martinez J, Pardo-Ibanez P. Adv. Mater. 2007; 19:1359.

19. Boldog I, Gaspar AB, Martínez V, Pardo-Ibanez P, Ksenofontov V, Bhattacharjee A, Gutlich P, Real JA. Angew. Chem. Int. Ed. 2008; 47:6433–6437.

20. Taylor KML, Jin A, Lin W. Angew. Chem. Int. Ed. 2008

21. Jung S, Oh M. Angew. Chem. Int. Ed. 2008; 47:2049–2051.

22. Rieter WJ, Taylor KM, Lin W. J. Am. Chem. Soc. 2007; 129:9852–9853. [PubMed: 17645339]

Biographies

Wenbin Lin obtained his BS and Ph.D. degrees from University of Science and technology of China (Hefei) in 1988 and the University of Illinois at Urbana-Champaign in 1994, respectively. After a NSF postdoctoral fellowship at Northwestern University, he became assistant professor of Chemistry at Brandeis University in 1997. He moved to the University of North Carolina at Chapel Hill in 2001, and was promoted to associate and full professor of chemistry in 2003 and 2007, respectively. His research focuses on designing novel molecular and supramolecular systems and hybrid nanomaterials for applications in chemical and life sciences.

William J. Rieter was born in Salisbury, MD, USA in 1982. He received a B.S. in biochemistry and a B.A. in chemistry from the College of Charleston in 2004. He was a NSF Predoctoral Fellow at the University of North Carolina at Chapel Hill, where he received his Ph.D. with Prof. W. Lin in 2008. He is currently pursuing a doctorate in medicine at the Medical University of South Carolina.

Kathryn M. L. Taylor was born in Upper Heyford, Oxfordshire, England in 1982. She received a B.S. in chemistry from the College of William and Mary in 2004. She is currently pursuing a doctorate in chemistry at the University of North Carolina at Chapel Hill with Prof. Wenbin Lin. Her current research is focused on the development of hybrid nanoparticles for biomedical applications.
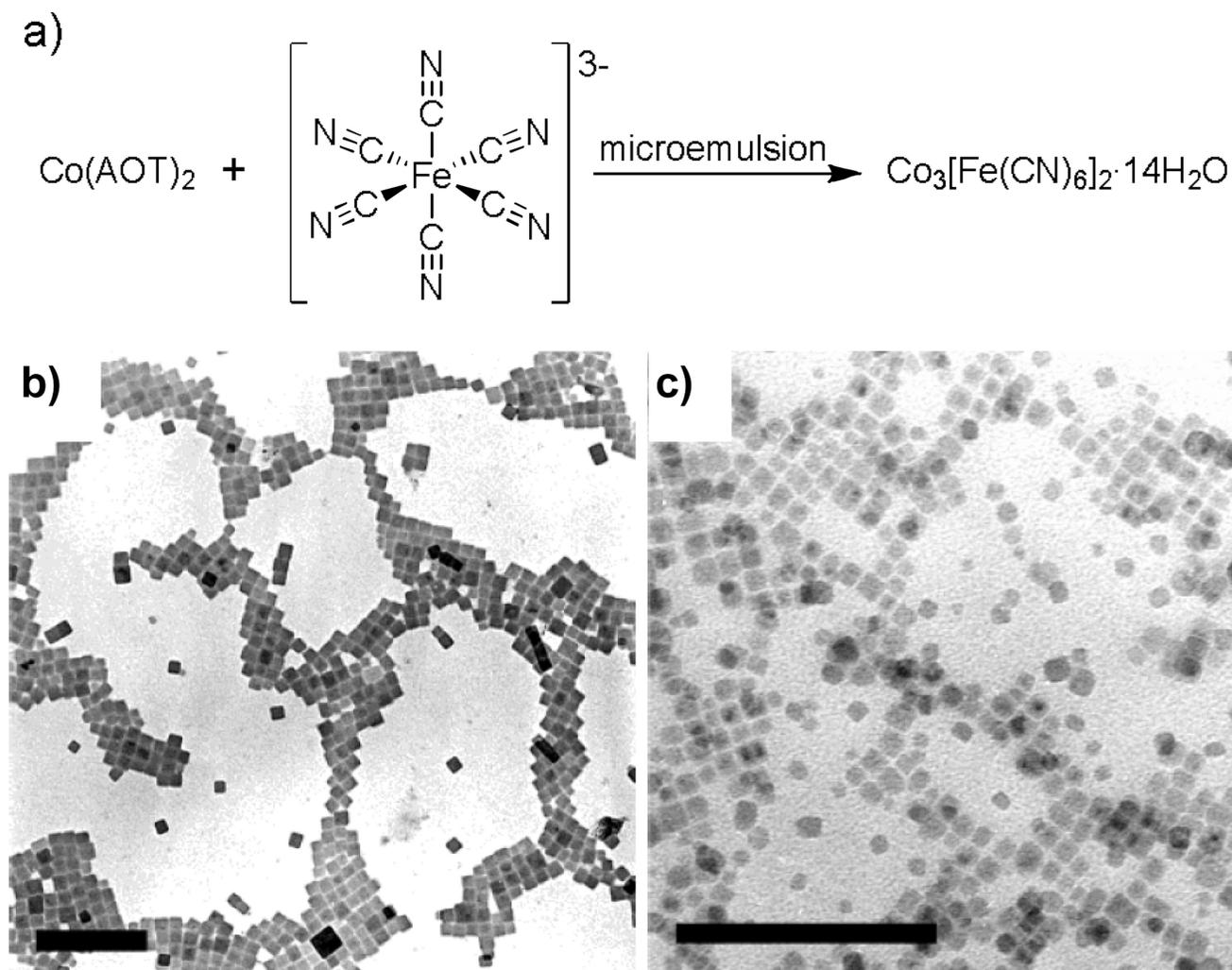
Figure 1.
a) Scheme illustrating the synthesis of cyanometallate nanoparticles. TEM images of cyanometallate nanoparticles synthesized in Co(AOT)$_2$ water-in-oil microemulsions at (b) *W* = 30 and (c) *W* = 10.[7b] Sacle bar = 200 nm. AOT is sodium bis(2-ethylhexyl) sulphosuccinate whereas *W* is the water to surfactant molar ratio.
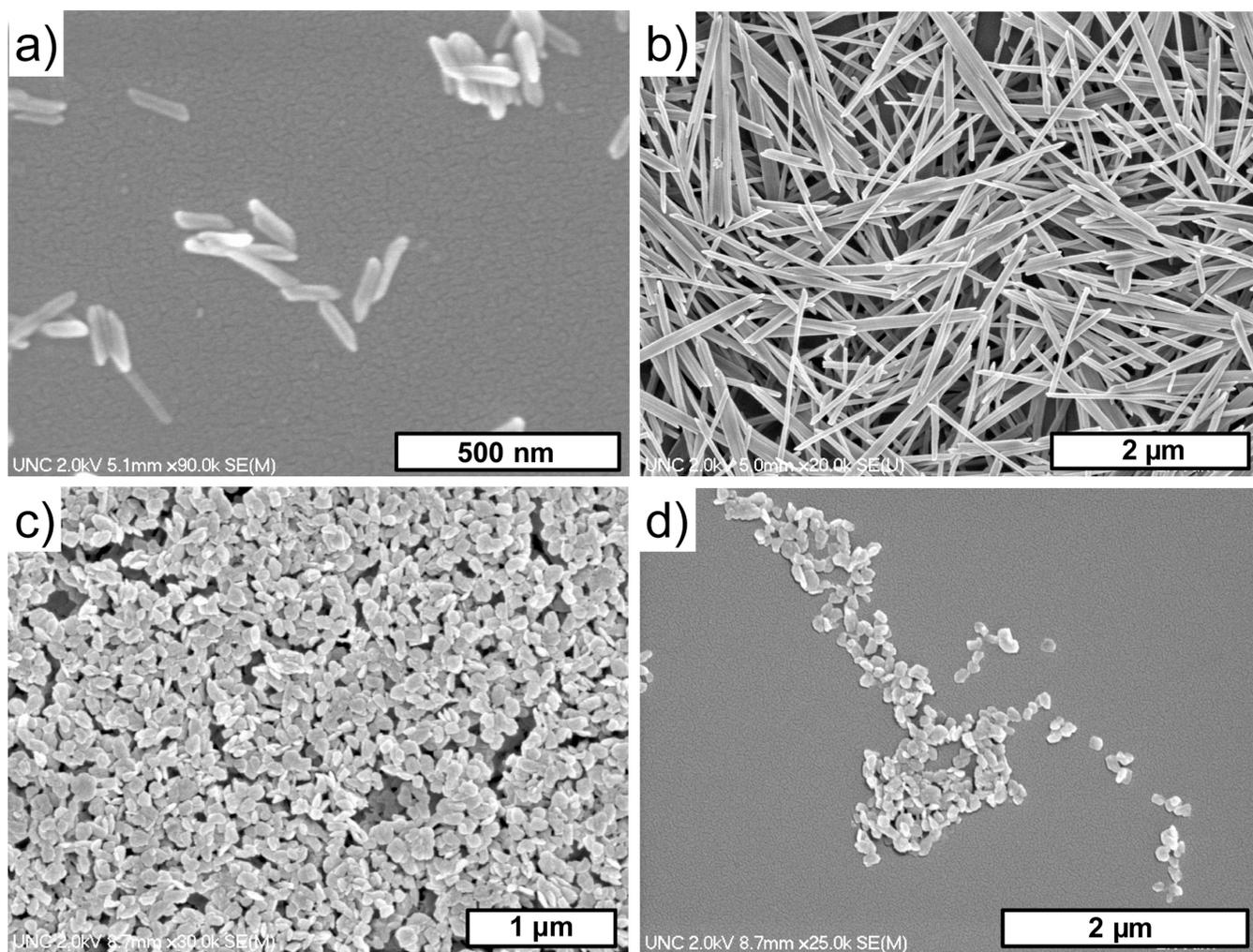
Figure 2.
a) Scheme for the synthesis of valence-tautomeric nanoparticles. b) SEM and (c) TEM micrographs of valence-tautormeric nanoparticles.[15]
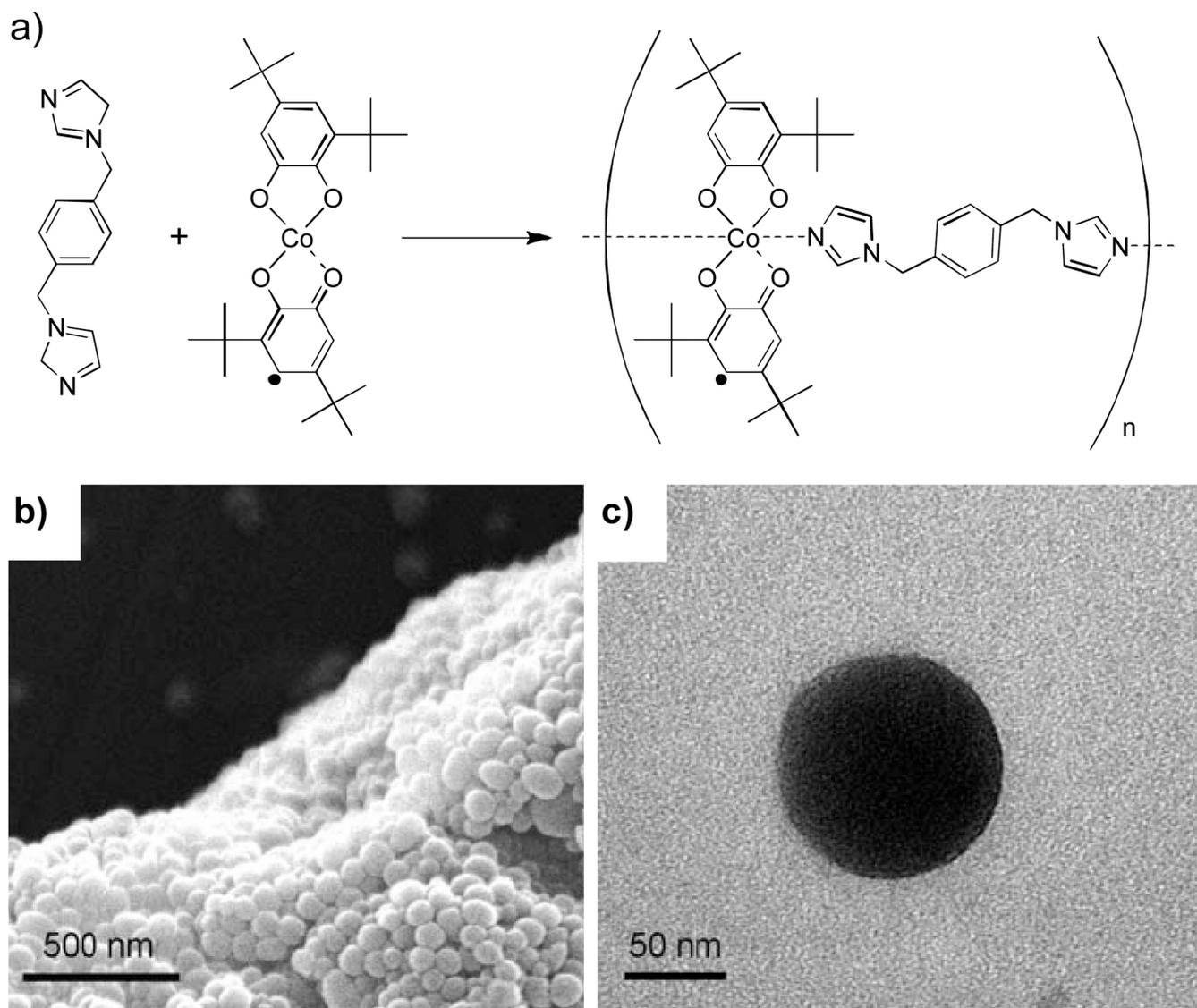
Figure 3.
SEM micrographs of $Gd_2(BDC)_3(H_2O)_4$ nanoparticles synthesized using a reverse microemulsion with (a) $W = 5$ and (b) $W = 10$. (c–d) SEM micrographs of [Gd(*i*BTC)$(H_2O)_3$]·H_2O.[16]
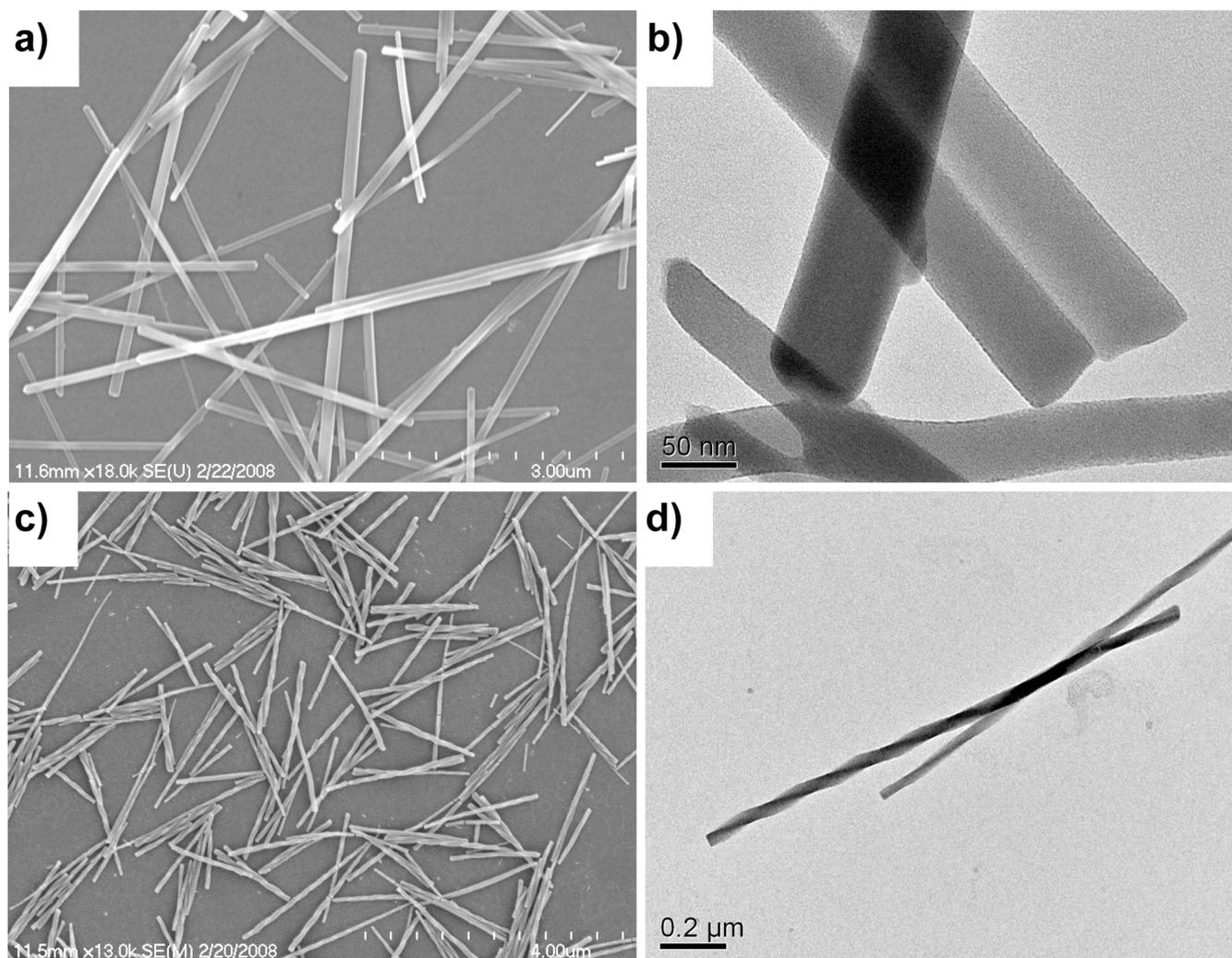
Figure 4.
(a) SEM and (b) TEM micrographs of crystalline $Mn(BDC)(H_2O)_2$. (c) SEM and (d) TEM micrographs of crystalline $Mn_3(BTC)_2(H_2O)_6$.[17]
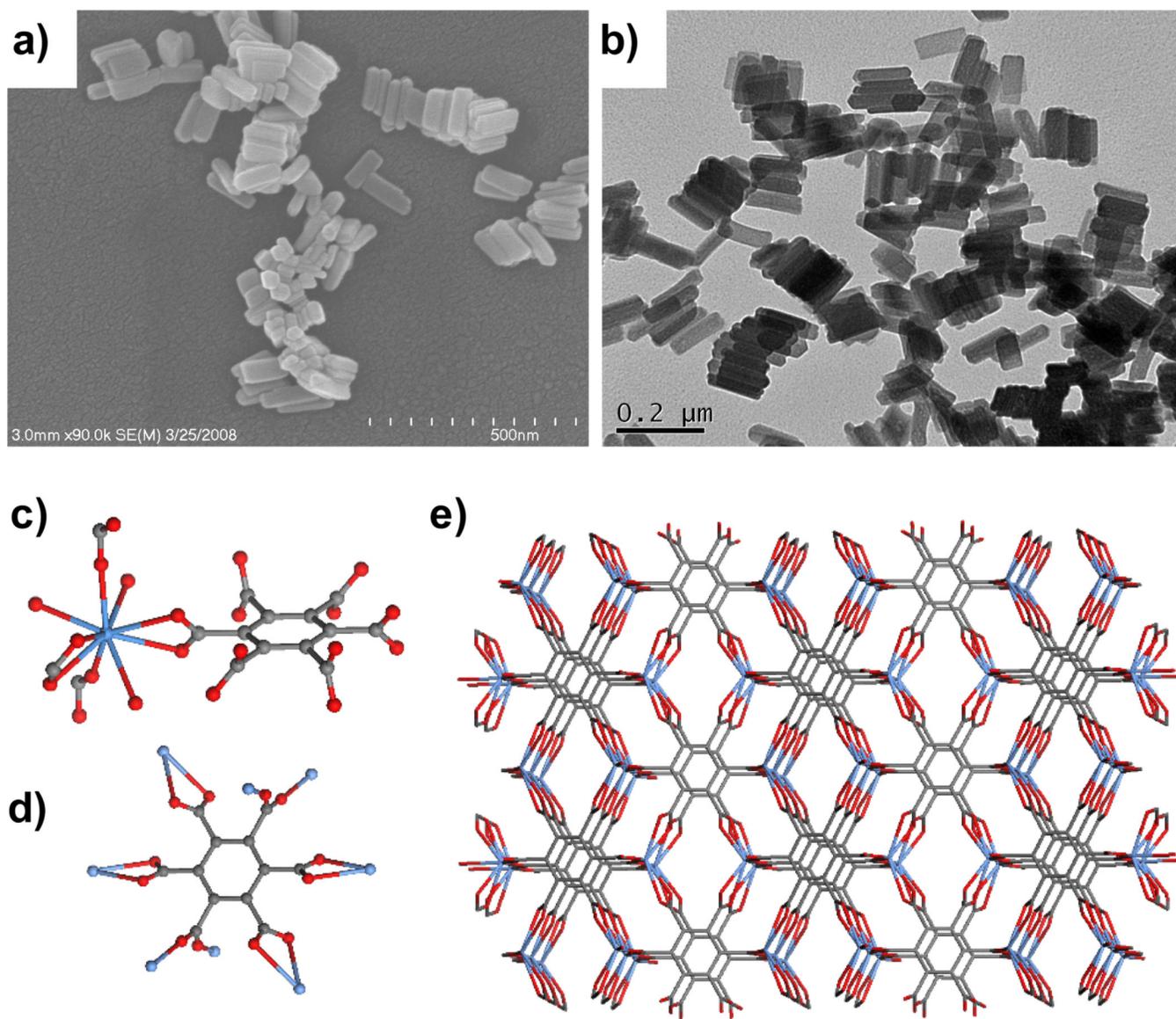
Figure 5.
(a) SEM and (b) TEM micrographs of $Gd_2(BHC)(H_2O)_6$. Crystal structures illustrating the (c) Gd coordination environment, (d) linking of BHC to eight different Gd centers, and (e) packing in $Gd_2(BHC)(H_2O)_6$. Structures were drawn using the cif file for isostructural $La_2(BHC)(H_2O)_6$.[20]
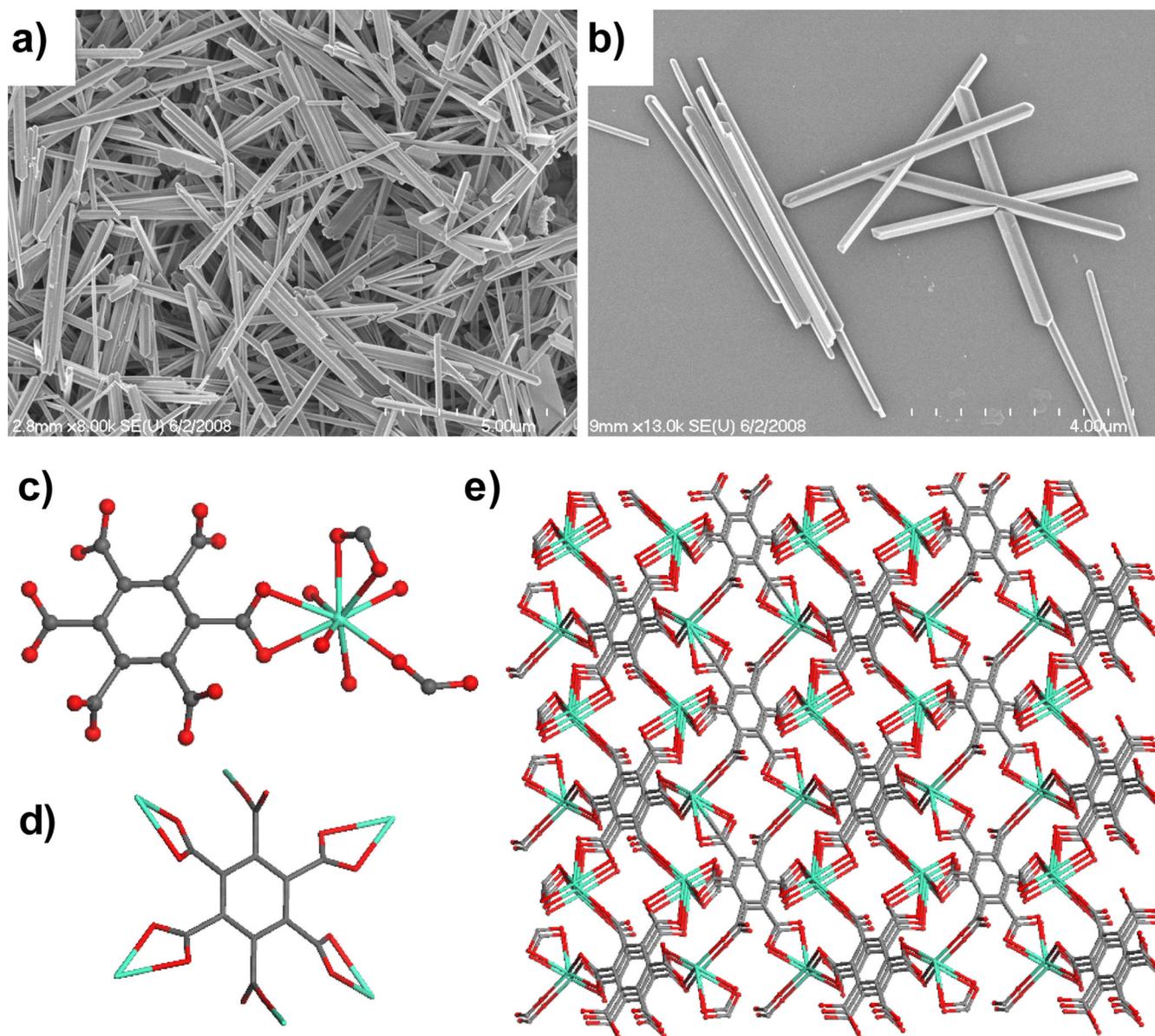
Figure 6.
(a–b) SEM micrographs of $[Gd_2(BHC)(H_2O)_8]\cdot 2H_2O$. Crystal structures illustrating the (c) Gd coordination environment, (d) linking of BHC to eight different Gd centers, and (e) packing in $Gd_2(BHC)(H_2O)_8]\cdot 2H_2O$.[20]
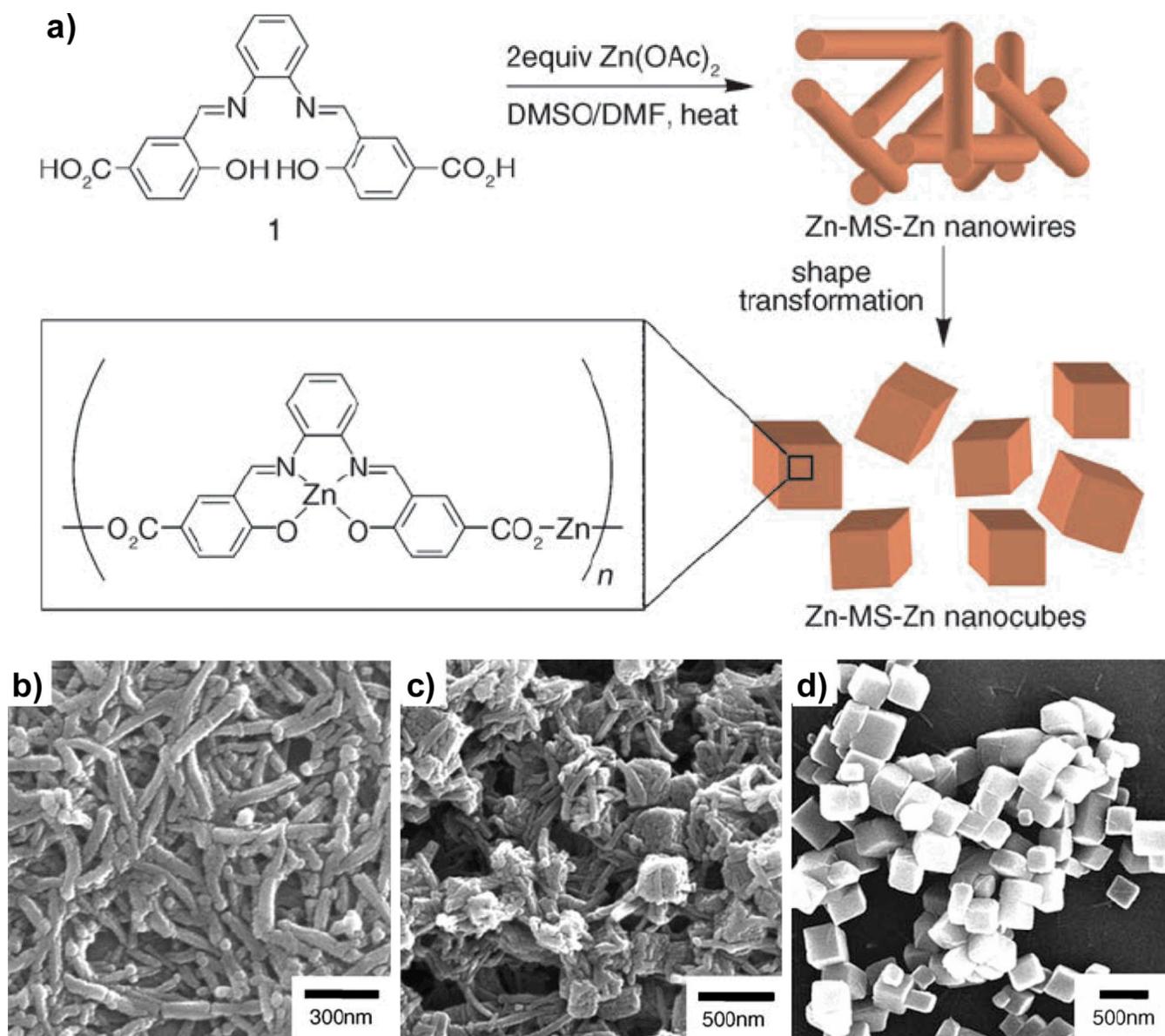
Figure 7.
(a) Scheme for the synthesis of Zn-MS-Zn nanowires and their subsequent transformation into nanocubes. (b–d) SEM micrographs illustrating the transformation of nanowires into nanocubes during the synthesis.[21]
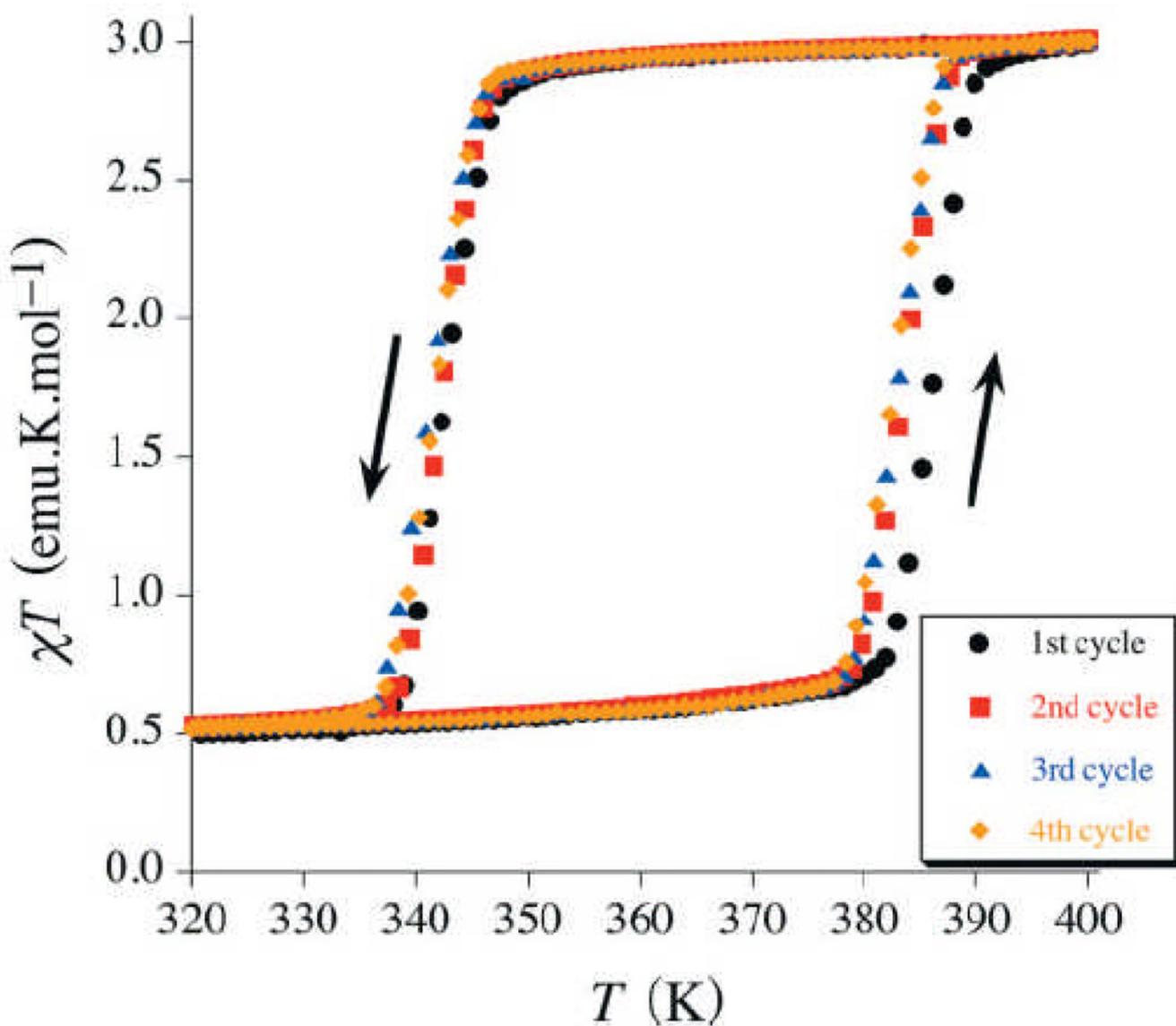
Figure 8.
Magnetic thermal hysteresis for [Fe(Htrz)$_2$(trz)](BF$_4$) nanoparticles.[18]
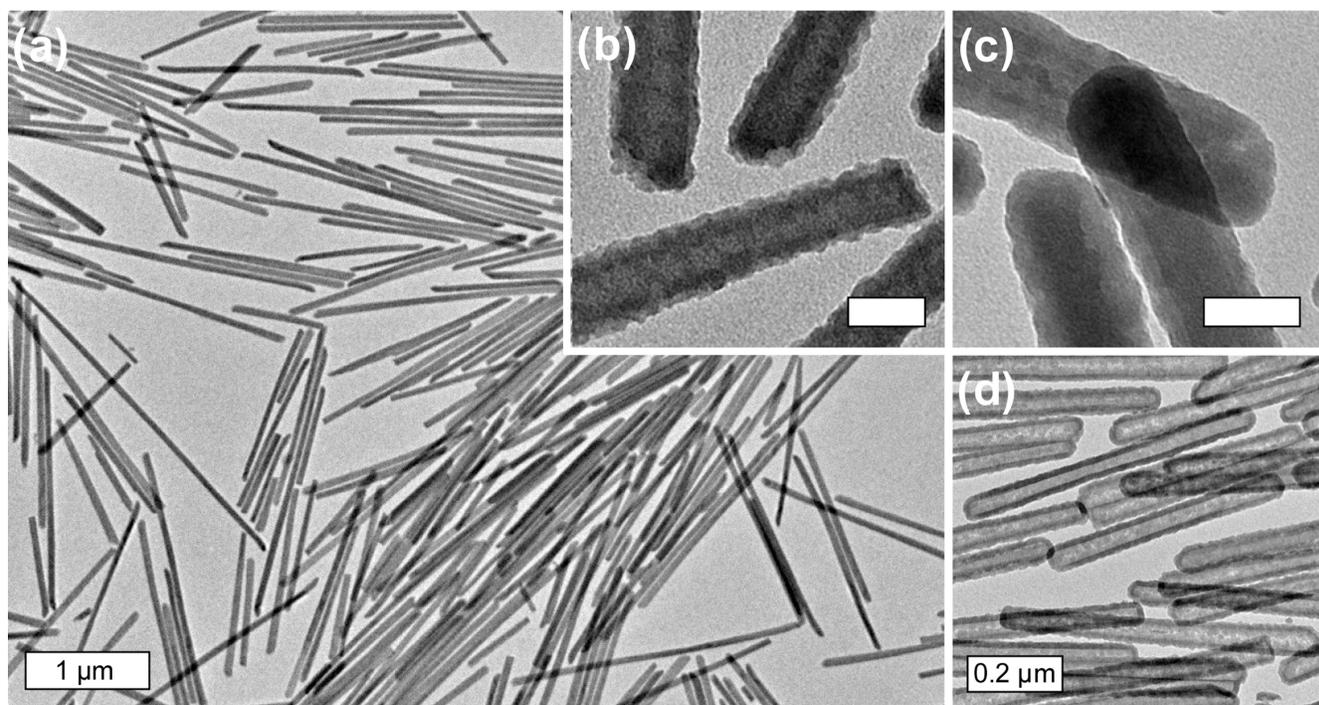
Figure 9.
(a and b) TEM images of $Gd_2(BDC)_3(H_2O)_4$ NMOFs with a 2–3 nm silica shell; (c) TEM image of $Gd_2(BDC)_3(H_2O)_4$ NMOFs with an 8–9 nm silica shell; (d) TEM image of 8–9 nm silica nanoshells generated from (c). Scale bars are 50 nm unless otherwise indicated.[22]
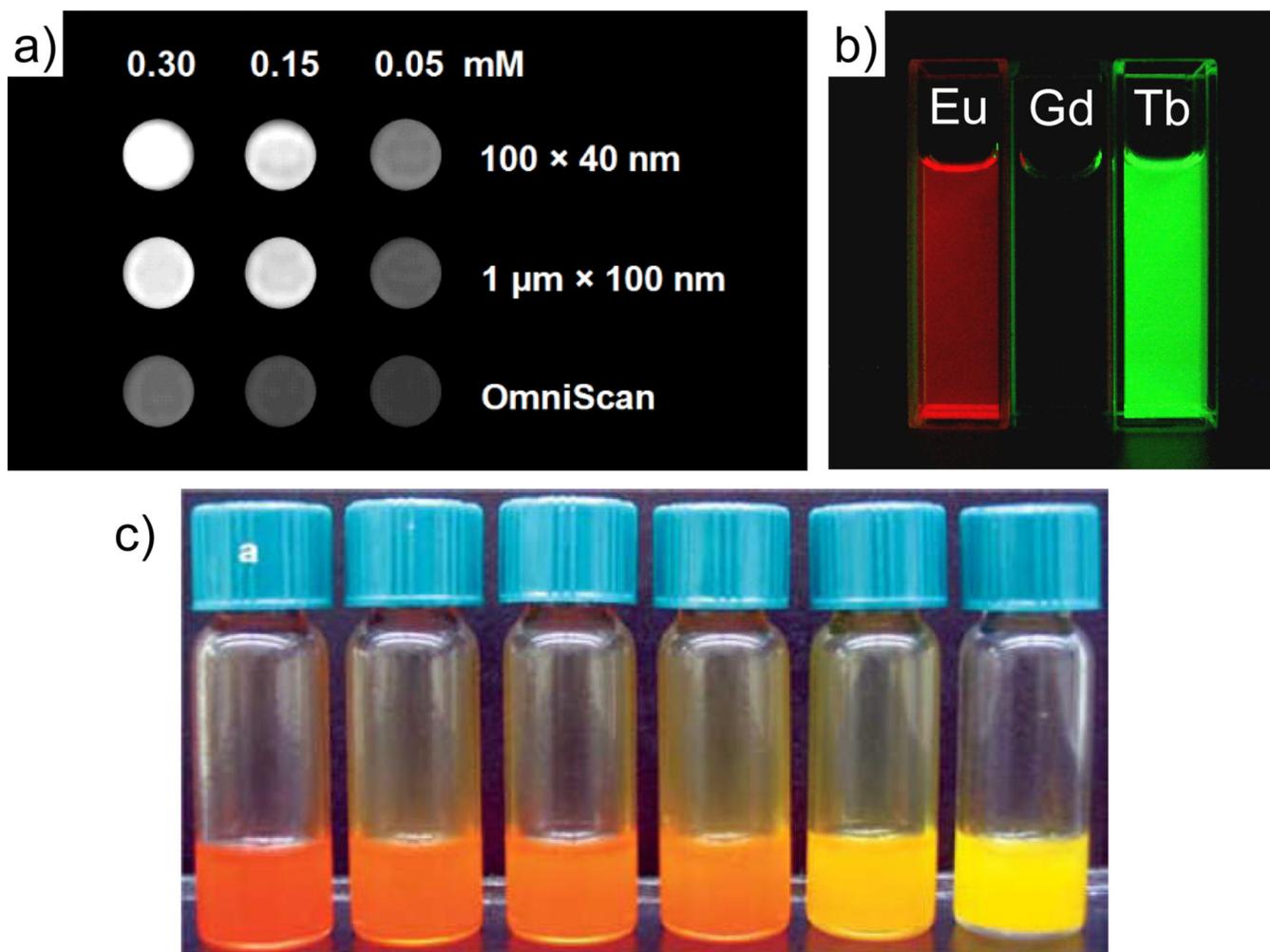
Figure 10.
(a) T_1-weighted MR phantom images of suspensions of $Gd_2(BDC)_3(H_2O)_4$ NMOFs in water containing 0.1 % xanthan gum as a dispersing agent. (b) Luminescence of ethanolic dispersions of Eu- and Tb-doped $Gd_2(BDC)_3(H_2O)_4$ NMOFs when irradiated with UV light.[16] (c) Luminescence of a series of Zn-BMSB-Zn particles in toluene with different ancillary ligands.[12]
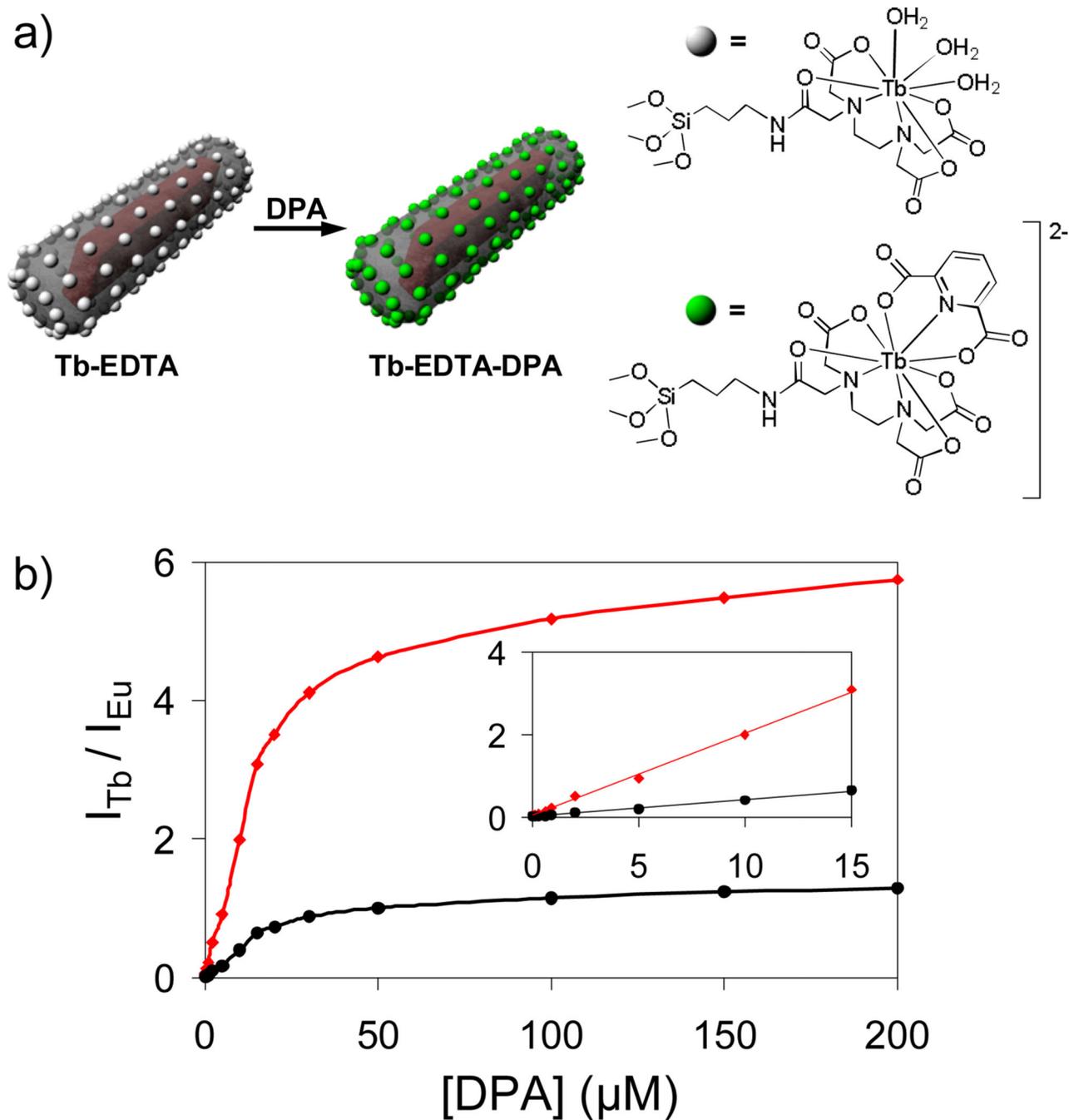
a)

b)

Figure 11.
(a) Schematic showing luminescence sensing of dipicolinic acid using core-shell nanostructures. (b) Ratiomeric curves obtained by plotting the Tb to Eu luminescence signal intensities exhibited by Tb-EDTA functionalized $Gd_{1.96}$:$Eu_{0.04}(BDC)_3(H_2O)_4$ against DPA concentration (red = 544 nm/592 nm, black = 544 nm/615 nm). The inset shows the linear relationship at low DPA concentrations.[22]
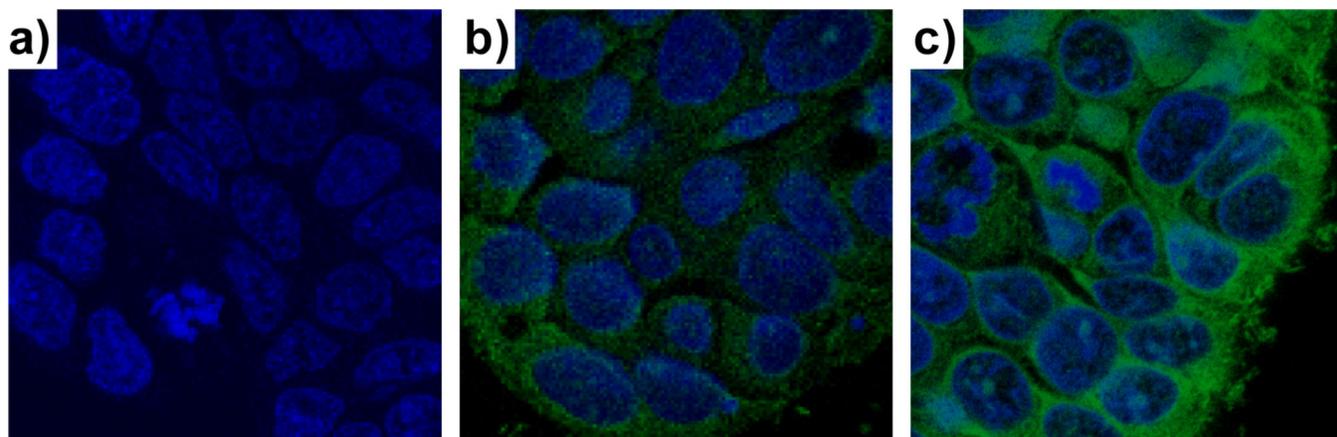
Figure 12.
Merged confocal images of HT-29 cells that were incubated with (a) no $Mn_3(BTC)_2(H_2O)_6$/silica core-shell nanostructures, (b) non-targeted $Mn_3(BTC)_2(H_2O)_6$/silica core-shell nanostructures, (c) c(RGDfK)-targeted $Mn_3(BTC)_2(H_2O)_6$/silica core-shell nanostructures. The blue color was from DRAQ5 used to stain the cell nuclei while the green color was from rhodamine B.
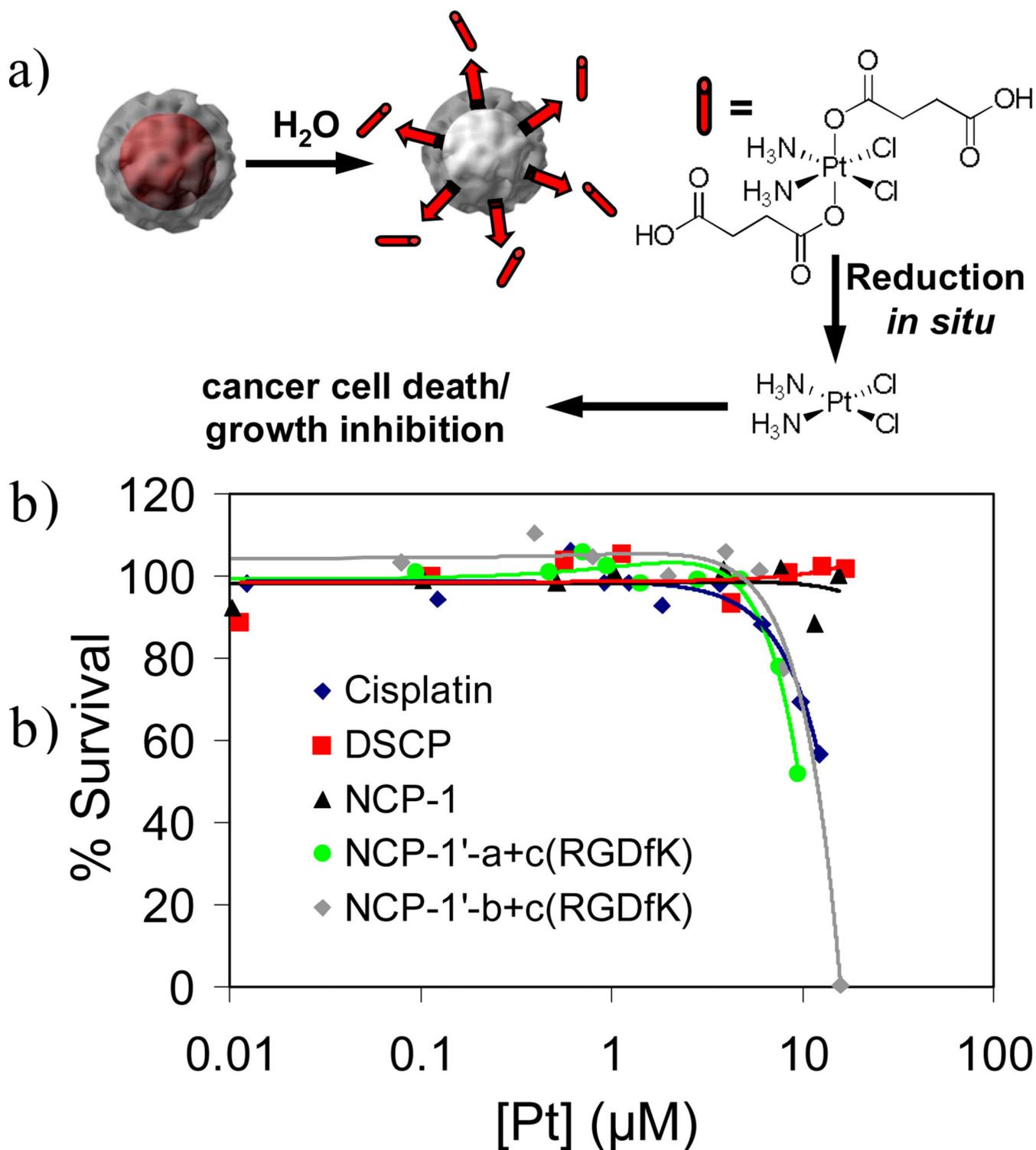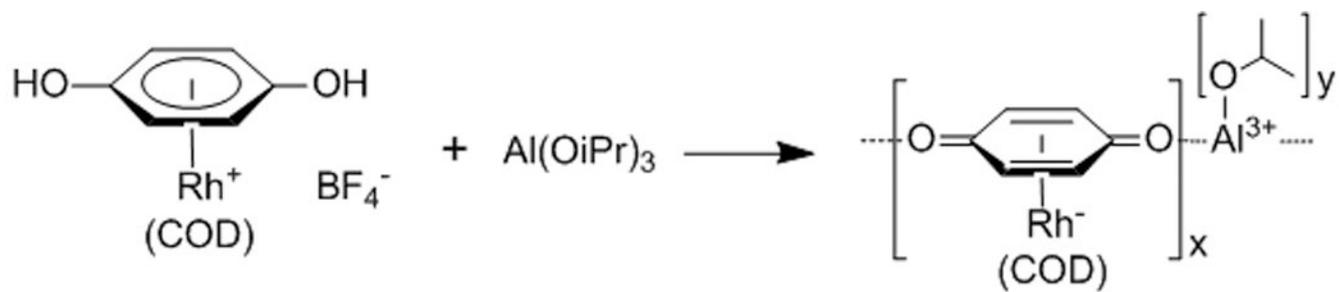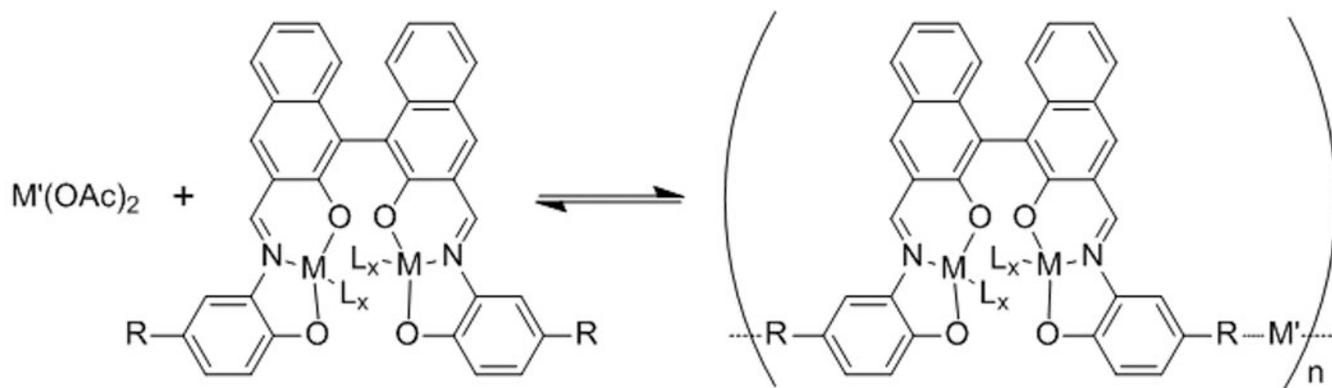
Figure 13.
(a) Schematic showing controlled release of DSCP from the core-shell nanostructure. (b) *In vitro* cytotoxicity assay curves for HT-29 cells incubated with various Pt-based NCPs.[13]
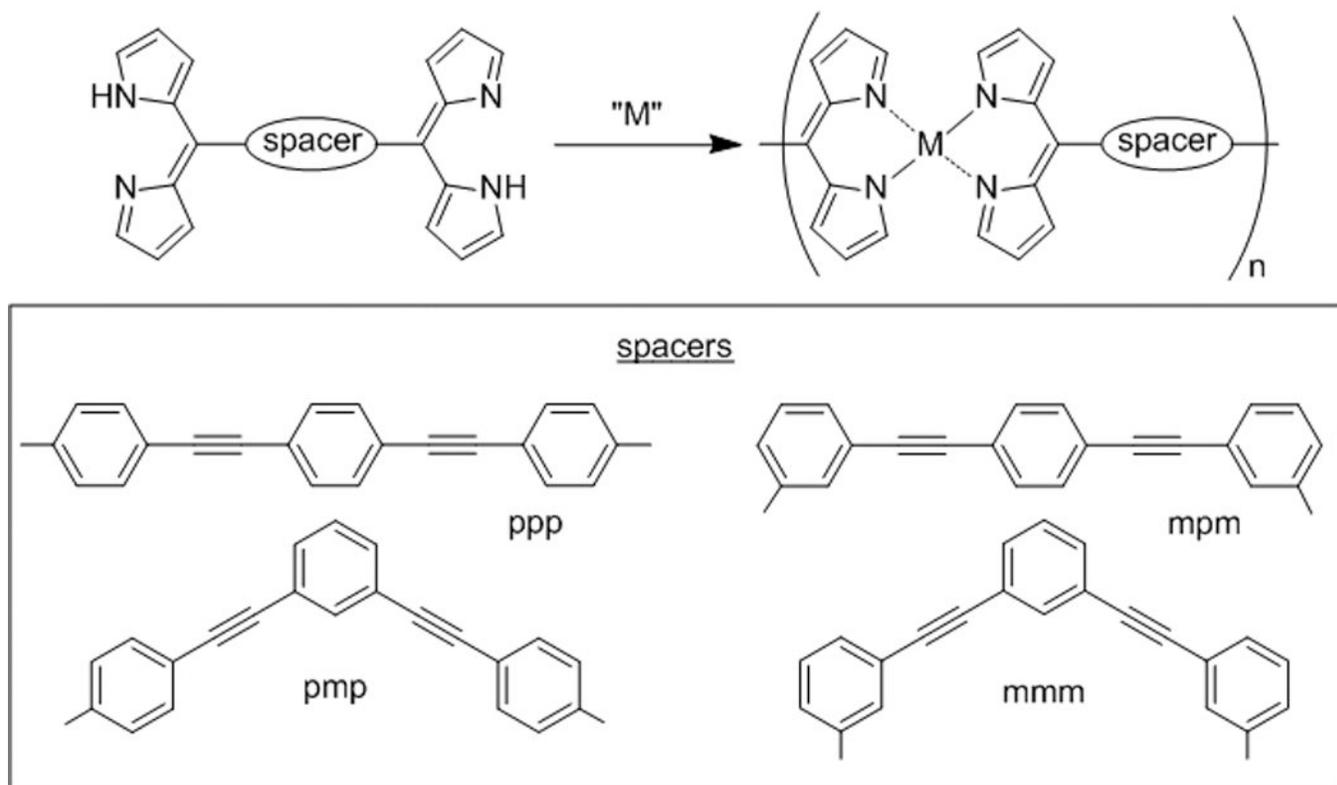
Scheme 1.
Synthesis of an organometallic nanocatalyst.[10]

Scheme 2.
Synthesis of NCPs based on the M-BMSB building block.[12]

Scheme 3.
Synthesis of NCPs based on the anticancer drug disuccinatocisplatin (DSCP).[13]

Scheme 4.
Examples of various dipyrrin "dimers" used to synthesize NCPs by Maeda et al.[14]

Table 1

Polymerization of phenylacetylene catalyzed by ONs.[10]

catalyst[a]	solvent	Mn	Mw/Mn	yield (%)
1+[a]	CH_2Cl_2	2900	1.8	90 (59)
ON1[b]	CH_2Cl_2	4100	4.3	82 (86)
ON2[c]	CH_2Cl_2	13200	3.4	84 (94)
ON3[d]	CH_2Cl_2	15600	3.5	86 (96)
1+	THF	17800	2.4	98 (59)
ON1	THF	23600	1.8	88 (95)
ON2	THF	26800	2.2	98 (95)
ON3	THF	29200	2.2	98 (96)

[a] $[(\eta^6\text{-}1,4\text{-hydroquinone})Rh(COD)]^+$

[b] 537 nm particles

[c] 402 nm particles

[d] 340 nm particles

Table 2

MR relaxivities for Gd- and Mn-based NMOFs synthesized by our group.[16],[17],[20]

	ion r_1	ion r_2
$Gd_2(BDC)_3(H_2O)_4$[a]	35.8	55.6
$Gd_2(BDC)_3(H_2O)_4$[b]	26.9	49.1
$Gd_2(BDC)_3(H_2O)_4$[c]	20.1	45.7
$[Gd(iBTC)(H_2O)_3]\cdot H_2O$	13.0	29.4
$Gd_2(BHC)(H_2O)_6$	1.5[d]	122.6[d]
$Mn(BDC)(H_2O)_2$	5.5	7.8
$Mn_3(BTC)_2(H_2O)_6$	7.8	70.8

All relaxivities were obtained at 3.0 Tesla and are given in $mM^{-1} s^{-1}$.

[a]Nanoparticle size was ~100 × 40 nm.

[b]Nanoparticle size was ~400 × 70 nm.

[c]Nanoparticle size was ~1000 × 100 nm.

[d]Values obtained at 9.4 Tesla.